IEEE Access
Multidisciplinary ⋮ Rapid Review ⋮ Open Access Journal

Received May 23, 2021, accepted May 30, 2021, date of publication June 4, 2021, date of current version June 15, 2021.

Digital Object Identifier 10.1109/ACCESS.2021.3086624

A YOLOv3 Deep Neural Network Model to Detect Brain Tumor in Portable Electromagnetic Imaging System

AMRAN HOSSAIN[1], (Member, IEEE),
MOHAMMAD TARIQUL ISLAM[1], (Senior Member, IEEE),
MOHAMMAD SHAHIDUL ISLAM[1], (Graduate Student Member, IEEE),
MUHAMMAD E. H. CHOWDHURY[2], (Senior Member, IEEE),
ALI F. ALMUTAIRI[3], (Senior Member, IEEE),
QUTAIBA A. RAZOUQI[3], (Member, IEEE), AND
NORBAHIAH MISRAN[1], (Senior Member, IEEE)

[1]Department of Electrical, Electronic and Systems Engineering, Faculty of Engineering and Built Environment, Universiti Kebangsaan Malaysia, Bangi 43600, Malaysia
[2]Department of Electrical Engineering, Qatar University, Doha, Qatar
[3]Electrical Engineering Department, Kuwait University, Kuwait City 13060, Kuwait

Corresponding authors: Amran Hossain (amranhossain38@gmail.com), Mohammad Tariqul Islam (tariqul@ukm.edu.my), and Ali F. Almutairi (ali.almut@ku.edu.kw)

This work was supported by Universiti Kebangsaan Malaysia, Malaysia.

ABSTRACT This paper presents the detection of brain tumors through the YOLOv3 deep neural network model in a portable electromagnetic (EM) imaging system. YOLOv3 is a popular object detection model with high accuracy and improved computational speed. Initially, the scattering parameters are collected from the nine-antenna array setup with a tissue-mimicking head phantom, where one antenna acts as a transmitter and the other eight antennas act as receivers. The images are then reconstructed from the post-processed scattering parameters by applying the modified delay-multiply-and-sum algorithm that contains 416×416 pixels. Fifty sample images are collected from the different head regions through the EM imaging system. The images are later augmented to generate a final image data set for training, validation, and testing, where the data set contains 1000 images, including fifty samples with a single and double tumor. 80% of the images are utilized for training the network, whereas 10% are used for validation, and the rest 10% are utilized for testing purposes. The detection performance is investigated with the different image data sets. The achieved detection accuracy and F1 scores are 95.62% and 94.50%, respectively, which ensure better detection accuracy. The training accuracy and validation losses are 96.74% and 9.21%, respectively. The tumor detection with its location in different cases from the testing images is evaluated through YOLOv3, which demonstrates its potential in the portable electromagnetic head imaging system.

INDEX TERMS Tumor detection, YOLOv3 model, data augmentation, electromagnetic imaging.

I. INTRODUCTION

Globally, brain tumor is one of the major causes of mortality and disability because it invades the most vital organ of the human body. A brain tumor is the growth of abnormal cells that have formed inside the head. At present, brain cancer is the 10th leading cause of death due to tumors for men and women [1]. Brain tumors can be deadly, significantly impacting the quality of life and changing everything for patients and their loved ones. A high death percentage is caused due to the invasive properties of tumors. But it is inspiring that the survival rate might increase if the diagnosis is performed at the early stage. In medical science, the standard imaging technologies to identify the tumor are computed tomography (CT) scans, MRI (magnetic resonance imaging) scanning, positron emission tomography (PET), ultrasound screening, and X-ray screening [2], [3]. The major pitfalls of the traditional imaging technologies are ionizing

The associate editor coordinating the review of this manuscript and approving it for publication was Giovanni Angiulli.

radioactivity, lower susceptibility, growing cancerous hazard, more expensive, etc. [3]–[8]. Nowadays, the possibility of electromagnetic imaging technology for the detection of brain tumors is gradually increased because of its special features like noninvasive, inexpensive, nonionizing radiation, and safe for the human body compared to the traditional technologies [9]–[12]. The antenna plays a significant role in the EM imaging system by producing EM waves. In EM imaging system, it is essential to design wideband antennas which will work within the frequency range of 1 to 4 GHz with high gain, and unidirectional characteristics [2], [9], [13]–[16]. A numerous number of EM imaging systems have been developed over time by applying the different types of antenna array [2], [9], [12], [17]–[19]. These systems use different types of imaging algorithm to detect brain tumor [2], [12], [14], [16]–[23]. An EBG-based microstrip patch antenna-based head imaging platform was presented in [11] to detect tumor. The system has no scanning process, and it uses a single antenna and confocal algorithm for imaging purposes. The system can detect only a single tumor along with the skull due to the lack of effectiveness of the algorithm. In addition, the system created noisy images due to the low bandwidth of the antenna and deficiency of the head scanning process. So, it is challenging to detect the tumor from the generated noisy images. A single 3D wideband antenna-based EM imaging system was developed to detect brain tumors [24]. The antenna's operating bandwidth is very low. The system produced blurry image due to very low bandwidth and coupling mismatch among the antennas as well as it is hard to identify the exact tumor location in the images. A unidirectional 3D antenna array-based system was developed to detect brain tumors by applying the DAS algorithm [25]. The used antenna and the imaging platform are very large. The measurement result from the system might be abnormal because of image slicing scenario. Besides identify the brain stroke in EM images, a single antipodal Vivaldi antenna-based head imaging system was presented in [15]. The system used only a single antenna with a low gain and DAS (delay-and-sum) image processing algorithm. As a result, it generates a low resolution-based noisy image caused by low gain and low operating bandwidth of the antenna. The imaging system is not able to detect the stroke at the central and depth position of the brain. In addition, a conformal wideband antenna-based head imaging system was developed to monitoring the stroke by processing S-parameters [17]. The system used multistatic delay-multiply-and-sum (DMAS) imaging algorithm. For imaging purposes, the system collects scattered (S-parameters) data from the thirteen antennas array. However, the system is not able to detect the stroke at the central and in-depth location due to lack of unidirectional characteristics phenomena of the antenna. A head imaging system with ten bowtie patch antennas array was developed and presented in [18]. The system collects scattered data (S-parameters) from the ten different scanning positions of the head surrounding. The system used Gauss-Newton Iterative imaging algorithm to reconstruct the images. This imaging mechanism is very complex and not usable due to the large size of an imaging system. Moreover, an electromagnetic stroke imaging system was developed by the ten wideband-monopole antennas array, where the used antenna covered very low bandwidth [23]. The scheme used a linear imaging algorithm and used the liquid as a testing phantom to generate images. As a result, the system produces noisy image, and hence hard to detect exact stroke location in the generated images. A twenty-four low-complexity triangular microstrip patch antennas array-based stroke imaging system was presented in [16]. Experimental system and imaging results were not presented in the literature. A compact 3D antenna was proposed for an electromagnetic head imaging system to detect brain stroke [13]. Only simulated imaging system with an eight antennas array are explained in the literature. But simulated imaging result with tumors was not described. Also, a three-dimensional (3D) slotted-folded dipole antenna-based stroke imaging system was implemented and explained in [19]. The system consisted of a vast sixteen antennas array and used the DAS algorithm for stroke imaging. The used algorithm is processed from S-parameters to generate the desired images, but it generates noisy images due to the lack of effectiveness of the algorithm. So, identification of the accurate stroke location in the image is complicated. Furthermore, a 3D dipole metamaterial loaded antenna-based head imaging system was developed to identify the stroke location and presented in [12]. A modified DMAS algorithm is used to detect stroke in the images.

Nowadays, deep learning technique (DLT) fascinates many attentions and has been used in medical imaging applications [26]–[29]. At present, researchers are motivated to apply this technique in electromagnetic imaging applications due to its abundant features [22], [30]–[32]. It can classify the target objects by training the convolutional neural networks (CNNs). It is noted that the deep learning approach with an optimization algorithm can solve the electromagnetic scattering discrepancy to enhance the image classification and help to detect the object from the generated EM images [33]. Classification of EM images and object detection is a challenging task due to the variation in features, algorithms, architecture, and training mechanism [27], [34]–[36]. A CNN architecture based on a super-resolution algorithm for microwave imaging is proposed in [37]. The architecture used a 33×33 image data set for training the network and produced 2D images. The generated images are noisy due to the lack of training data set. Therefore, identification of the accurate location of the object in the image is tricky. An automated brain tumor classification approach is demonstrated in [29]. Wavelet transform and principal component analysis (PCA) techniques are used for feature extraction and DNN (deep neural network) to classify tumors. Still, the classification accuracy was very low because of the deficiency of training samples. The EM image reconstruction process by the deep learning approach is presented in [30]. The approach used 24×24 antenna array, auto-encoder, and decoder for reconstructing the images. In addition, 32000 images

(each image size was 128 × 128 pixels) were used for reconstructing the microwave image, but they did not demonstrate the object detection development. A brain tumor segmentation by the LinkNet [38] framework method is presented in [22]. The classification of tumors in the brain based on the MRI image data set is presented, but the tumor detection procedure is not analyzed. An automatic brain tumor detection and segmentation using a fully convolutional network (F-CNN) approach are demonstrated in [39]. In this approach, the U-net framework [32] with Adam optimization algorithm was used for segmentation of the image regions. From the segmentation, the tumor could be detected, but the accurate location of the tumor in the image is difficult to identify due to the shortage of unbiased predictor. A residual deep neural network approach is used to classify and detect the tumor in the head [28]. The approach used data distillation and augmentation methods to reduce the noise label in the image, but detection scenario with experimental analysis is not performed. Therefore, deep neural network-based object detection model could be a new research finding for brain tumor detection with accurate localization in EM imaging systems.

It is noteworthy to mention that the reported head imaging system used various conventional imaging algorithms to detect tumor from the reconstructed images, but it is challenging to identify the accurate location of the tumor due to the low spatial resolution. In addition, it is very much challenging to detect and localize the tumor from the reconstructed images for the non-expert physician or patients. Moreover, it is often confused by the physician if the reconstructed images are noisy and blurry. Therefore, it is essential to indicate the tumor locations manually by the expert physician, which is a crucial drawback of the conventional EM imaging system. Thus, the motivation towards overcoming the issue in the reported EM head imaging system relies on a deep neural network model that can automatically detect and localize the tumor from the scanned head region.

In this article, we present a deep neural network based YOLOv3 algorithm to detect tumor with their location in the human brain. The main contributions of this research can be stated below:

i) To the best of the authors' knowledge, this is the first work, where the deep learning technique is applied to detect the target brain tumor and its location in EM head images.
ii) Developed a new portable EM head imaging system by using a compact three-dimension (3D) unidirectional, high bandwidth wideband antennas array to generate high resolution-based EM images.
iii) Implemented a darknet-53 deep neural network-based YOLOv3 algorithm that able to automatically detect tumor and their location, including bounding boxes in generated EM images.
iv) The outcome of this research is verified by EM image visualization and evaluated tumor detection performances by applied different sizes of training and testing data set.

The YOLOv3 algorithm is based on darknet-53 deep neural network architecture, which is applied to identify the target tumor in the EM images. The algorithm is implemented by using the Python programming language with TensorFlow API. An experimental portable electromagnetic head imaging system is implemented for imaging purposes. Electromagnetic head images with tumor objects are generated by applying the modified delay-multiply-and-sum image processing algorithm [12]. The single image contains 416 × 416 pixels. Fifty sample images from different scenarios are collected through the developed EM imaging system. Furthermore, the image augmentation method is used to produce the final data set that will later be used for training, validation, and testing purposes. The image data set consists of 1000 samples with a single and double tumor. Later, eight hundred EM images are used for training the network, where one hundred are used for validation, and the rest one hundred are used for testing purposes. The tumor detection performances with different data sets are examined. It is shown that the detection accuracy was more than 95%, and F1 score was more than 94%, when considered maximum images as a training data set. In addition, the training Vs validation accuracy and training Vs validation loss are also demonstrated. The average training accuracy, training loss, validation accuracy, and validation loss are 96.74%, 14.01%, 98.84%, and 9.21%, respectively. Higher training accuracy, F1 score, and lower validation loss ensure better detection performances. Furthermore, tumor detection results in different scenarios (i.e., with sing and double tumors) are evaluated and presented. It is observed from the detection results that the tumor location with different sizes is successfully detected.

The rest of the paper is organized as follows: Experimental validation of the EM imaging system is presented in section II. Detailed analysis of the deep neural network-based YOLOv3 model is demonstrated in section III. In section IV, the procedure of training, validation, and testing of the images are presented. Then, results and discussions are presented in section V, and finally, the concluding statements are in section VI.

II. EXPERIMENTAL VALIDATION OF EM SYSTEM

A wideband antenna is required in an EM head imaging system within the range of 1 GHz to 4 GHz with unidirectional radiation characteristics. A 3D antenna is designed and fabricated on cost-effective Rogers RT5880 substrate material, where the dielectric constant is 2.20, the loss tangent is 0.0009, and the thickness is 1.575 mm. The optimized antenna dimension is 53 × 22 × 21.575 mm^3. The scattering parameters $|S_{11}|$ are measured by the power network analyzer (PNA). The simulated and measured scattering parameters $|S_{11}|$ are illustrated in Figure 1(a). It can be observed that the measured operating frequency of the antenna is 1.43 GHz to 3.71 GHz, whereas the simulated operating frequency of

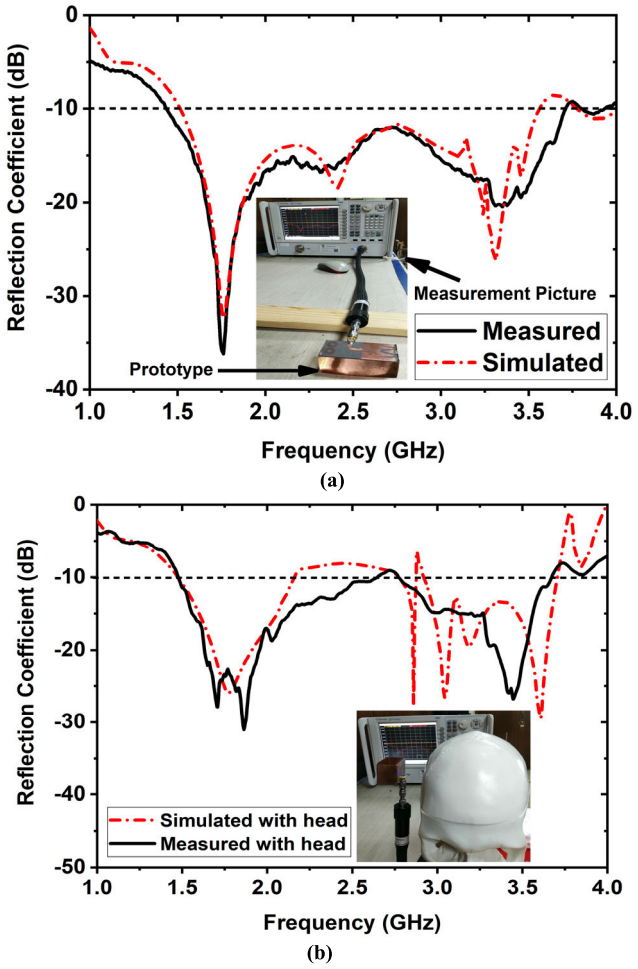

FIGURE 1. Simulated and measured results of the antenna: (a) Reflection coefficient in free space (b) Reflection coefficient with the head model.

the antenna is 1.51 GHz to 3.55 GHz, respectively. Later, the 3D antenna is simulated with a Hugo head model and measured with a fabricated head phantom model to evaluate the performance stability of the antenna. The simulated and measured reflection coefficient curves with a head model are depicted in Figure 1(b).

It is notable that the reflection coefficient of the antenna in head proximity maintains good agreement between the simulated and measured results. An experimental setup is developed to validate the performance of the antenna and tissue-mimicking head phantom, which is later utilized to reconstruct the tumor images. The overall experimental imaging setup is depicted in Figure 2(a). The imaging setup consists of nine 3D antennas array, where the gap between each antenna is 40 mm. The distance of every antenna from the centre of the top rotating disk is 100 mm, and the angle of the antenna-to-antenna centre point is 40°. The antenna positions are numerically indicated by the green color in Figure 2(a). Antenna 1 acts as a transmitter. The remaining eight antennas are acted as receivers for receiving the scattering signals. The mounted antenna array system is rotated by the stepper motor from 0 to 2π around the fabricated

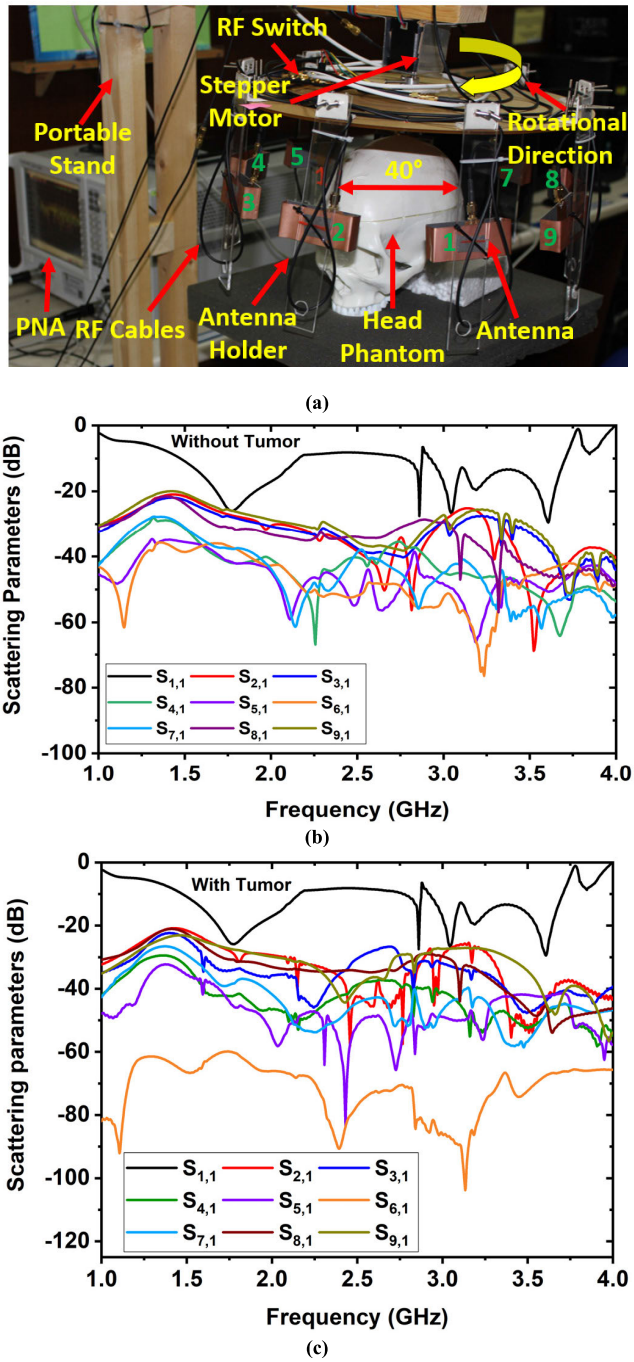

FIGURE 2. (a) Developed EM head imaging system (b-c) scattering parameters.

head phantom. Figure 2(b-c) depicts the scattering parameters (i.e., with and without tumor) of each antenna. The backscattered signals (S2, 1, S3, 1, S4, 1, S5, 1, ... S9, 1) are collected in every 7.2 degrees rotation. Therefore, the total $9 \times 8 \times 50$ locations are scanned to assess and generate high-resolution images. Later, the collected backscattered signals are post-processed by the modified delay-multiply-and-sum frequency domain image algorithm [12] to reconstruct the images of head regions. Figure 3 represents the tissue-mimicking phantom and the reconstructed images of

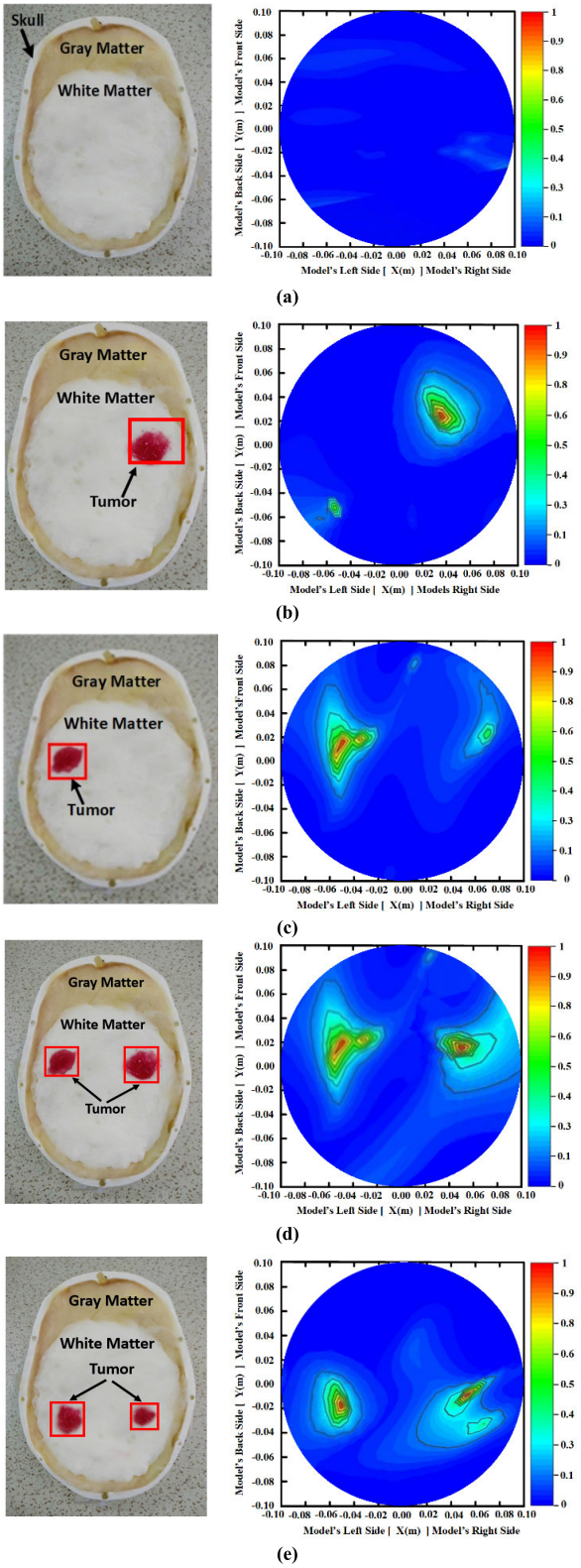

FIGURE 3. Fabricated tissue-mimicking head phantom and reconstructed images (a) Reconstructed blank image (without tumor) (b-c) two different configurations of the same phantom with single and (d-e) two different configurations of the same phantom with double tumors.

the head region, where the phantom is used inside the head model to validate the overall system's performance.

For instance, one blank tissue-mimicking head model configuration without tumor and the corresponding reconstructed image is illustrated in Figure 3(a). In addition, two different configurations with the single and double tumor in the same head phantom model are shown in Figure 3(b-e), respectively. In Figure 3(b-e), the right-side images are reconstructed images of the corresponding phantom model configurations. The horizontal (x-axis) and vertical (y-axis) axis scaling of each image in this article is considered as -0.10 meter (m) to $+\ 0.10$ meter (m). The coordinate $\{0.00,0.00\}$ represents the centre position of the head model. The tissue layers of the phantom and a tumor are fabricated by the following recipe presented in [40]. The different fabricated size of the tumor is measured as the diameter D = 10mm, 12mm, 14mm, 15mm, 18mm, 20mm, 22mm and 25 mm. For imaging purposes, a single tumor in a different location is used in twenty-five samples and double tumors in different locations are used in another twenty-five samples. Consequently, a total of fifty samples of reconstructed images are collected afterwards to create an original image data set. Furthermore, the created data set is applied to train the deep learning object detection model. Later, the YOLOv3 object detection model is utilized to detect the tumor location from the generated reconstructed images. The model is implemented by applying the Python programming language with a TensorFlow API.

III. THEORETICAL BACKGROUND

A. YOLOv3 ALGORITHM ANALYSIS

YOLO (You only look once) is one of the state-of-the-art real-time object detection algorithms developed by Joseph Redmon *et al.* [41]. Currently, YOLO version 3 (YOLOv3)[42] is a super-fast latest object detection algorithm which is evolved from the YOLO [41] and YOLOv2 [43]. YOLOv3 comprises a single deep convolutional neural network (DCNN) that split the input image into a grid of cells, and every cell directly predicts a bounding box (BB) and object classification. The typical framework of YOLO is depicted in Figure 4. The main principle of the algorithm is to split the input image into an M $\times$ M grid and make predictions in every grid cell. Moreover, if the

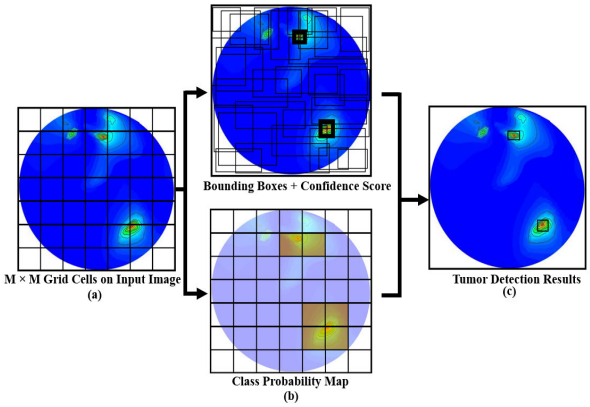

FIGURE 4. YOLOv3 model with the object detection method.

centre location of an object is found in a grid cell, that grid is liable for identifying that object. Every grid cell predicts B bounding boxes with the confidence scores for those boxes. In addition, these confidence scores reflect whether an object presents in the grid cell or not, and it reflects the box is that it predicts accurately. In general, the confidence score is calculated by the following equation:

$$Confidence = P_r(Object) \times IoU(GrountTruth,\ PredBox) \tag{1}$$

where $P_r(Object) \in \{0, 1\}$, IoU represents the intersection over the union between the GroundTruth (GT) and predicted box (PredBox). However, the confidence score should be $\{1\}$, if no object exists in that cell, otherwise the confidence score (C) is equal to the intersection over union $\{IoU\}$ between the GT and PredBox. Also, every cell predicts C conditional class probabilities for the detecting object. Thus, total $(5 + C)$ values are expected by every cell those are: $\{x, y, w_i, h_i, confidence\}$ and C conditional class probabilities. In this case, $\{x, y\}$ denote the centre position coordinates of the box, and $\{w_i, h_i\}$ denote the width and height of the box, respectively. YOLOv3 solved different types of issues in YOLOv2, including batch normalization problems, skip connection issues and localization precision issues. In addition, YOLOv3 predicts objects in three different scales, which are accurately given by the downsampling (DS) the input image sizes by 32, 16, and 8, respectively. Thus, it might be remedying the object size variation issues. However, the prediction is encoded in YOLOv3 as follows:

$$M \times M \times (B \times 5 + C) \tag{2}$$

where $M \times M$ is the grid cell of the input image, B is the number of bounding boxes in a cell, "5" is for the attributes of 4 bounding boxes and one object confidence, and C denotes the number of classes. Since a target object can belong to several classes, so, one 1×1 convolutional layer and a logistic regression activation function are used instead of the SoftMax layer. The confidence score of every class is projected through logistic regression, and the target object is detected by a threshold value. However, the error between the predicted value and real value is usually computed by three loss functions such as: classification loss, localization loss, and confidence loss. The final cross-entropy loss function with the combination of three loss functions as follows [44]:

$$\begin{aligned} Loss = {} & \lambda_{coord} \sum_{i=0}^{S^2} \sum_{j=0}^{B} \mathrm{I}_{ij}^{obj} \\ & \times \left[\left(\sigma(t_x)_i^j - \sigma(\hat{t}_x)_i^j \right)^2 + \left(\sigma(t_y)_i^j - \sigma(\hat{t}_y)_i^j \right)^2 \right] \\ & + \lambda_{coord} \sum_{i=0}^{S^2} \sum_{j=0}^{B} \mathrm{I}_{ij}^{obj} \left[\left(t_{w_i^j} - \hat{t}_{w_i^j} \right)^2 + \left(t_{h_i^j} - \hat{t}_{h_i^j} \right)^2 \right] \\ & + \sum_{i=0}^{S^2} \sum_{j=0}^{B} G_{ij} \left(C_i^j - \hat{C}_i^j \right)^2 \\ & + \lambda_{nobj} \sum_{i=0}^{S^2} \sum_{j=0}^{B} \mathrm{I}_{ij}^{nobj} \left(C_i^j - \hat{C}_i^j \right)^2 \\ & + \sum_{i=0}^{S^2} \mathrm{I}_{ij}^{nobj} \sum_{c \in classes} \left(p_i^j(c) - \hat{p}_i^j(c) \right)^2 \end{aligned} \tag{3}$$

where I_{ij}^{obj} represents that, when the j^{th} bounding box of the i^{th} grid cell is responsible for predicting the target object, and the value is equal to 1; otherwise, it is 0. The S^2 represents the number of grid cells, and B represents the number of bounding boxes in every grid cell. The offsets of the centre locations are represented by the $\sigma(t_x)$, and $\sigma(t_y)$. The component C represents the confidence score and p represents the probability of the target object class.

B. NON-MAXIMUM SUPPRESSION METHOD

The target objects in an image might be of various sizes and shapes, and to capture every of these perfectly. In YOLOv3 model creates multiple bounding boxes in an image for detecting target objects, as shown in Figure 4 (b), but for each target in the image, we must have a single bounding box, as shown in Figure 4(c). The Non-Maximum Suppression (NMS) method is a popular method that selects a single bounding box out of multiple overlapping bounding boxes for detecting the target objects in an image. It is used to eliminate redundant detections and discover the best match for final detection. The NMS algorithm is shown in **Algorithm 1.**

Algorithm 1 The Pseudocode of the Non-Maximum Suppression (NMS) Method

Input : $B = \{b_1, b_2, ..., b_N\}$, $C_S = \{c_1, c_2, ..., c_N\}$, T_h
B is the initial detection boxes;
C_S contains the corresponding detection confidence scores;
T_h is the *NMS* threshold;
Output: List of final detection boxes D;

```
D ← {}
while B ≠ ∅ do
    m = arg max C_S
    D ← D ∪ b_m; B ← B − b_m; C_S ← C_S − c_m
    for b_i ∈ Bdo
        if IoU (b_m, b_i) ≥ T_h then
            B ← B − b_i; C_S ← C_S − c_i
        end if
    end for
end while
```

IV. MATERIALS AND METHOD

A. PROCEDURE OF TRAINING, VALIDATION AND TESTING

This section analyzes the procedures of making the image data set for training, validation, and testing. Two types of image data sets are considered, which consist of reconstructed images with single and double tumors. Fifty samples of

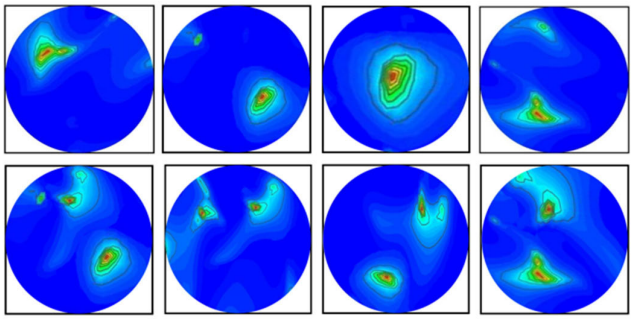

FIGURE 5. Collected sample reconstructed images with single and double tumors.

reconstructed images with single and double tumors are collected from the EM imaging system. The resolution of the reconstructed images is $416 \times 416 \times 3$ pixels.

Figure 5 depicts some of the sample reconstructed images with single and double tumors. It is noted that a YOLOv3 requires a large number of image data sets for the model to be trained effectively to detect the targeted object in the image. This assists in enhancing the performance of the model by simplifying reducing the overfitting. Thus, in this study, the image augmentation techniques are used on collected fifty samples to generate a large number of images as a final image data set for training purposes. The technique creates a rich, diverse set of images from the small sample image data set for image classification and object detection. There are eight augmentation techniques used by the python programming language for generating the final image data set such as: (i) rotation, (ii) scaling, (iii) cropping, (iv) zooming, (v) width shifting, (vi) height shifting, (vii) horizontal flipping, and (viii) vertical flipping. In the rotation case, angles for the augmentation technique are -10 to 10 degrees, -50 to 50 degrees, -70 to 70 degrees, -90 to 90 degrees, -130 to 130 degrees, and -180 to 180 degrees, respectively. As a result, target objects are shifted at different locations in the images. The random factor is in the range of 1.15 to 1.25 for the scaling and cropping of the images. Thus, the target object is also shifted at different locations. Moreover, 5% to 30% zooming are considered to demonstrate objects size (i.e., small size for lower percentage and large size for higher percentage) in the images. In addition, the width and height shifting range is between 10% to 30% to change the target object setting at different positions in the images. Besides, the images are vertically and horizontally flipped with a probability factor of 0.3 to 0.5 to shift the target object location at different places in the images. Programmatically, taking one sample from the original fifty (50) samples and then applied the above augmentation techniques to generate nineteen (19) images at a time. Consequently, $19 \times 50 = 950$ images are obtained for 50 samples. However, the final image data set consists of 1000 images with the original 50 samples, which are divided into three sets, including training set, validation set, and testing set. From that, 80% of the images are used as a training set, 10% images are used as a validation set, and the remaining 10% images are used as a testing set. Figure 6 depicts the randomly selected images from the augmented final image data set after the augmentation procedure. Since the YOLOv3 is a pre-trained model on MSCOCO (Microsoft Common Objects in Context) data set with 80 predefined classes, it uses darknet-53 convolutional neural network as a backbone of the model. The final image data set of the target object (i.e., tumor) as a class is not included in the predefined data set of YOLOv3. Therefore, in this study, the proposed final image data set is used as a class to the YOLOv3 model for training, validation, and testing purposes. Thus, an annotation file needs to be created for every image in the final image data set. The annotating process (i.e., YOLO labelling format) generates a text file with the same name for every image that contains the object class number, coordinates, height, and width. The annotation file for YOLO looks like the following format as a text file:

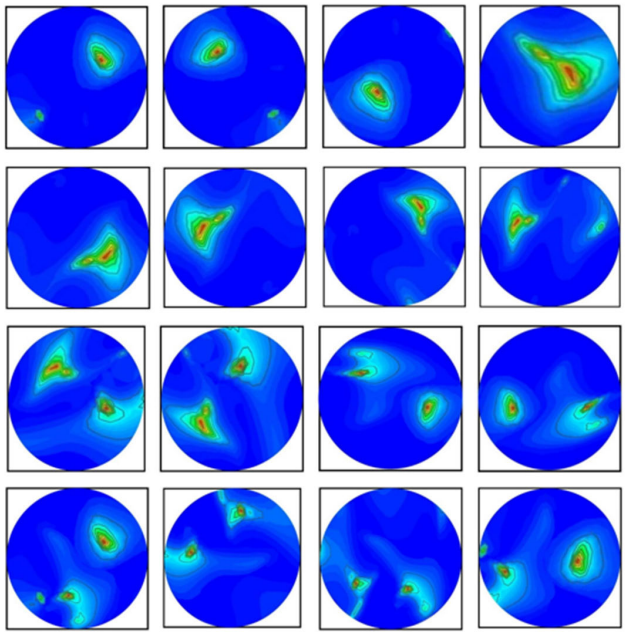

FIGURE 6. Randomly selected images from the augmented final image data set for training.

$$< \boldsymbol{object - class} >< \boldsymbol{x} >< \boldsymbol{y} >< \boldsymbol{width} >< \boldsymbol{height} >$$

Here, < object-class > denotes the class number, < x > and < y > denote the center x and y coordinates, and < width > and < height > denote the width and height of the target object in the images. Thus, an annotation tool is needed to label objects manually in the image by creating an annotation file. To create the annotation file, a graphical image annotation tool LabelImg is used on the custom augmented image data sets for labelling target objects (i.e., tumor location). The tool uniformly labels each target object (i.e., tumor) from the images in the training, validation, and testing set. Finally, all these files, including image files and text files, are considered the main image data sets, which are then used to train the network. For instance, the contents of the annotation file with

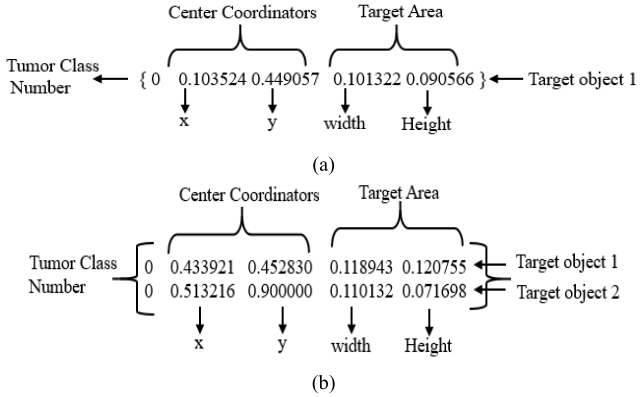

FIGURE 7. Example of contents of the annotation text file as YOLO format: (a) For single tumor object in an image (b) For double tumor objects in an image.

single and double tumor objects are shown in Figure 7. The file has mainly three indications of each target object (i.e., tumor) such as a tumor class number or id, tumor object's bounding box centre coordinate, tumor object's area. Here, tumor class means that every image of the custom dataset (i.e., Final image dataset for training) has only one class, which is the only tumor. Because in YOLOv3 dataset has predefined 80 classes (i.e., person, bicycle, car, motorcycle, airplane, bus, train, truck, boat, traffic light, fire hydrant, stop sign, parking meter, bench, bird, cat, dog, horse, ……., toothbrush) [42]. Since the tumor class does not exist in the predefined class of YOLOv3, so in this work, predefined 80 classes are ignored and used only a single tumor class-based custom dataset. Thus, the tumor class is mentioned in the annotation files, where the first column value "0" represents only a single tumor class number or id. The annotation file format of single tumor and double tumors object labelling information are presented in Figure 7(a) and Figure 7(b), respectively.

B. TUMOR YOLOv3

The YOLOv3 algorithm is an enhancement of the previous version of YOLOv2 and YOLOv1 algorithms. It has the benefits of accurate positioning, high detection accurateness, and high speed. Besides, it can achieve the detection of small target objects and decent robustness to environmental scenes. The YOLOv3 network architecture is shown in Figure 8. The input image dimension of the architecture is $416 \times 416 \times 3$, where height is 416 pixels, width is 416 pixels, and 3 represents the color (i.e., Red, Green, Blue) channel numbers of an image. This algorithm is based on Darknet-53 network architecture, which acts as a backbone of the YOLOv3. The Darknet-53 architecture in YOLOv3 uses a numerous number of 1×1 and 3×3 convolutional layers, so that connect local features interactions as well as its roles. It is a feature extraction network with 53 convolutional layers. Two convolutional kernels of 1×1 and 3×3 are used, where every layer's batch normalization (BN) layer is used for normalization purposes. In this architecture, the pooling layer is removed, and the Leaky ReLU activation function is used to enlarge the convolutional kernel's step size by diminishing the size of the feature map. Due to the deeper network characteristics of the Darknet-53, it has the enhanced feature extraction ability that detects small objects in the images. There are two sampling layers (Up Sampling) and three convolutional sets in the detection phase. A convolutional set consists of three 1×1 convolutional kernels and two 3×3 convolutional kernels. The sampling layer generates the small-size images through the interpolation of small-size properties maps and relative techniques. When connections are established among some layers to link the low-level characteristics with the high-level characteristics, the satisfactory-grained information of the high-level abstract features is improved. As a result, enhanced high-level abstract features might be used aimed at class prediction and bounding box (BB) regression. The YOLOv3 architecture prediction procedure is described below:

Step 1: At the beginning, the images of size 416×416 are applied as input to the Darknet-53 framework. After the execution of many convolutions, a 13×13 sized feature map is obtained. After that, seven times by 1×1, and 3×3 convolutional kernels are executed to obtain the first scale (scale 1) as well as regression BB prediction.

Step 2: In this stage, the 13×13 sized feature map is processed by a convolution set (i.e., contains three 1×1 and two 3×3 convolutional kernels), and then the convolutional process is executed by using a 1×1 convolutional kernel. Thereafter, by two times the sampling (upsampling), a 26×26 sized feature map is gained. After that, the new 26×26 sized feature map is performed seven times by 1×1 and 3×3 convolutional kernels to attain the 2nd scale (scale 2) and regression BB prediction.

Step 3: In this phase, the 26×26 sized feature map is processed by a convolution set (i.e., contains three 1×1 and two 3×3 convolutional kernels), and then the convolutional process is executed by using a 1×1 convolutional kernel. After that, by two times the sampling (upsampling), a 52×52 sized feature map is obtained. After that, the new 52×52 sized feature map is performed seven times by 1×1 and 3×3 convolutional kernels to achieve the third scale (scale 3) and regression BB prediction.

Step 4: In the final step, the feature maps of different sizes (i.e., 13×13, 26×26, 52×52) are optimized for detecting the small target objects with regression BBs. Hence, at every position, every feature map predicts 03(three) regression BBs, so there are $3 \times (13 \times 13, 26 \times 26, 52 \times 52) = 10647$ regression bounding boxes. However, predicted output with bounding boxes is displayed as a final target object detection result.

V. RESULTS AND DISCUSSIONS

A. EXPERIMENTAL PLATFORM, IMAGE DATA SET & NETWORK TRAINING

The YOLOv3 deep neural network model is implemented on the Windows10 OS with 128 GB RAM and 64-bit Intel(R) Xeon(R) W-2104 at the rate of 3.30 GHz CPU. The NVIDIA

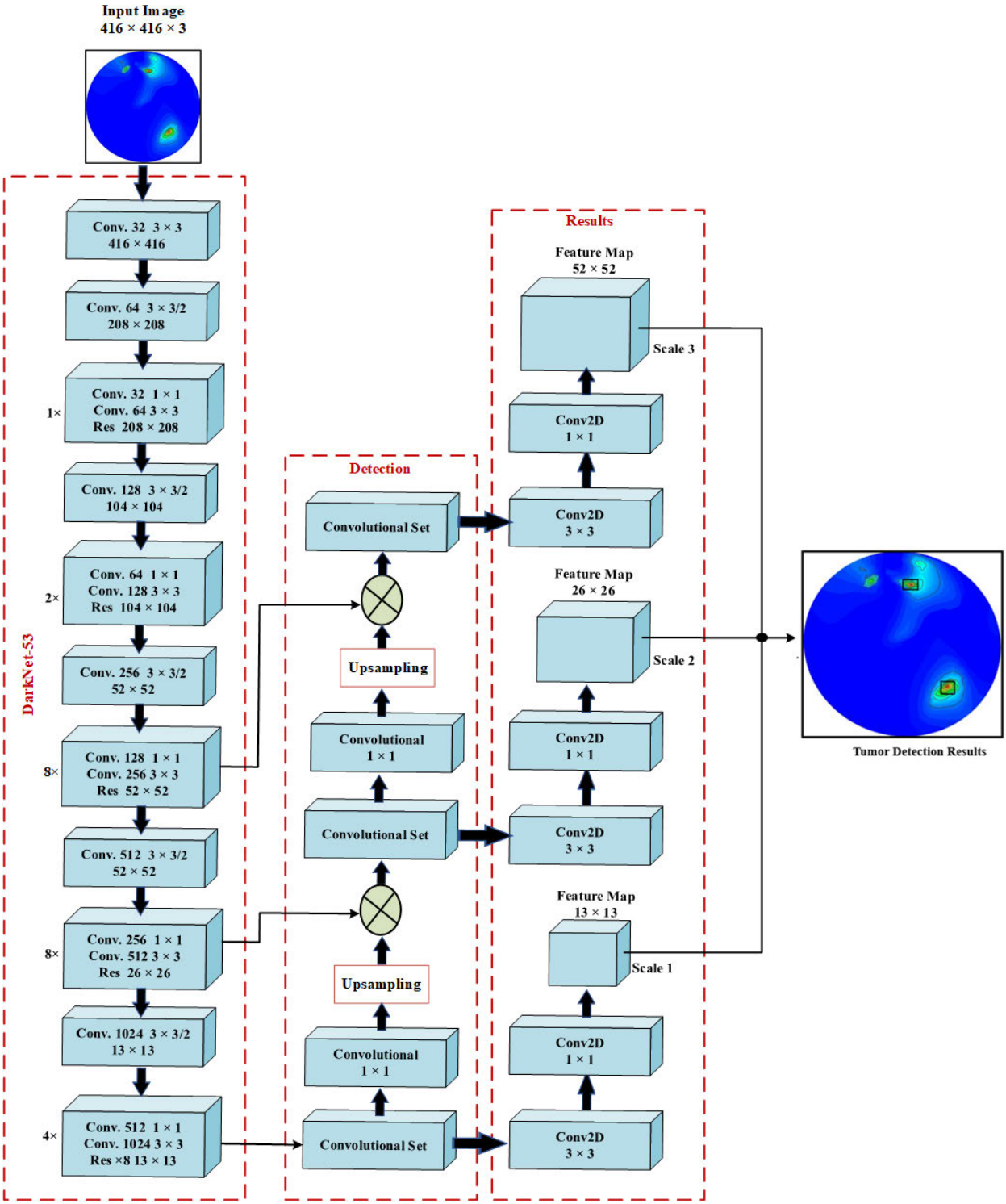

FIGURE 8. The YOLOv3 network architecture diagram for brain tumor detection.

GeForce GTX 1080Ti GPU is used to accelerate the training of the network. Under the Anaconda distribution platform, a jupyter notebook is used, and the program is written by the Python 3.7 version with TensorflowAPI (2.3.0 Version). The final image data set is used as inputs into the model. The data set consists of 1000 sample images, where 80% of them are used for training, 10% are used for validation, and the rest of 10% is used for testing purposes. In the training stage, we used the final image data set with their classification annotation files to the YOLOv3 model, and

the weight of Darknet-53 was restored as a classification network. The model is trained for 200 epochs with an initial learning rate of 0.001, then divided by ten (10) after 60 and 120 epochs. The adjustment of the learning rate increases the training accuracy and decreases the validation loss. The optimizer is momentum, and it is set to 0.9. The batch size and weight decay are set to 16 and 0.0005, respectively. After 20000 iterations, the model shows a better result for the provided images. As a result, the obtained loss and accuracy are 0.0921 and 0.9562, respectively.

For evaluating the effectiveness of the tumor detection, the data set from the proposed reconstructed images is utilized. Three evaluation parameters: Precision (P), Recall (R), and F1 score are applied to examine the trained YOLOv3 algorithm by following the equations.

$$P = \frac{N_{TP}}{N_{TP} + N_{FP}} \tag{4}$$

$$R = \frac{N_{TP}}{N_{TP} + N_{FN}} \tag{5}$$

$$F_1 = \frac{2 \times R \times P}{R + P} \tag{6}$$

Here, P represents the precision rate of the tumor, N_{TP} represents the number of correctly detected tumors, N_{FP} represents the number of samples with tumor detection errors, R represents the recall rate of the tumor, and N_{FN} represents the number of tumor samples from the missed detection.

The NMS threshold (T_h) value is fixed to 0.48. So, when the intersection (IoU) ratio between the predicted BB and the accurate location of the tumor object is greater than 0.48, the tumor could be detected appropriately. The evaluation of different parameters is performed by the different training data set on tumor detection, which is presented in Table 1. It is concluded that the performance evaluation of the YOLOv3 detection model improves with the increment of the training data set size.

TABLE 1. The detection performance parameters with different training data sets.

Training Data set	Precision (%)	Recall (%)	F1(%)
200	53.62	51.41	52.49
400	84.63	82.48	83.54
600	91.33	90.23	90.77
800	95.62	93.41	94.50

B. EXPERIMENTAL DATA ANALYSIS

This section discusses the impact of the training data set on the training and validation accuracy with their loss. After completing the model's training with different training data set, including 200, 400,600, and 800 images, it is validated by the validation data set. The training and validation accuracy graph with respect to epochs is depicted in Figure 9. It can be observed that when the model is trained by 200 images, its validation accuracy shows very low values. Besides, when the model is trained by 400 images, its validation accuracy is increased, but it slightly decreases in different epochs.

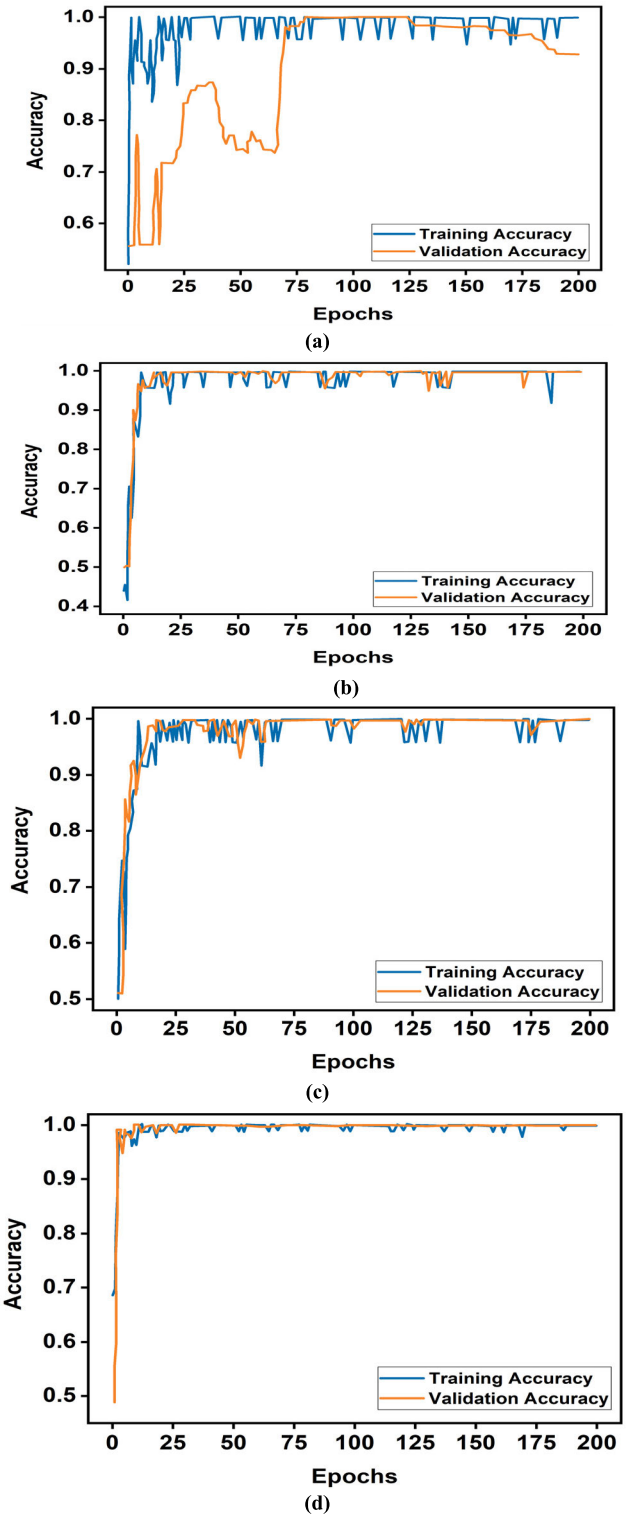

FIGURE 9. Training Vs validation accuracy: (a) For 200 images data set (b) 400 images data set (c) 600 images data set (d) 800 images data set.

In addition, when the model trained by the 600 images, its validation accuracy was higher than the validation accuracy of 400 images, whereas when the model is trained by the 800 images, its validation accuracy was 100% from the epochs 40-200. In addition, the training and validation loss

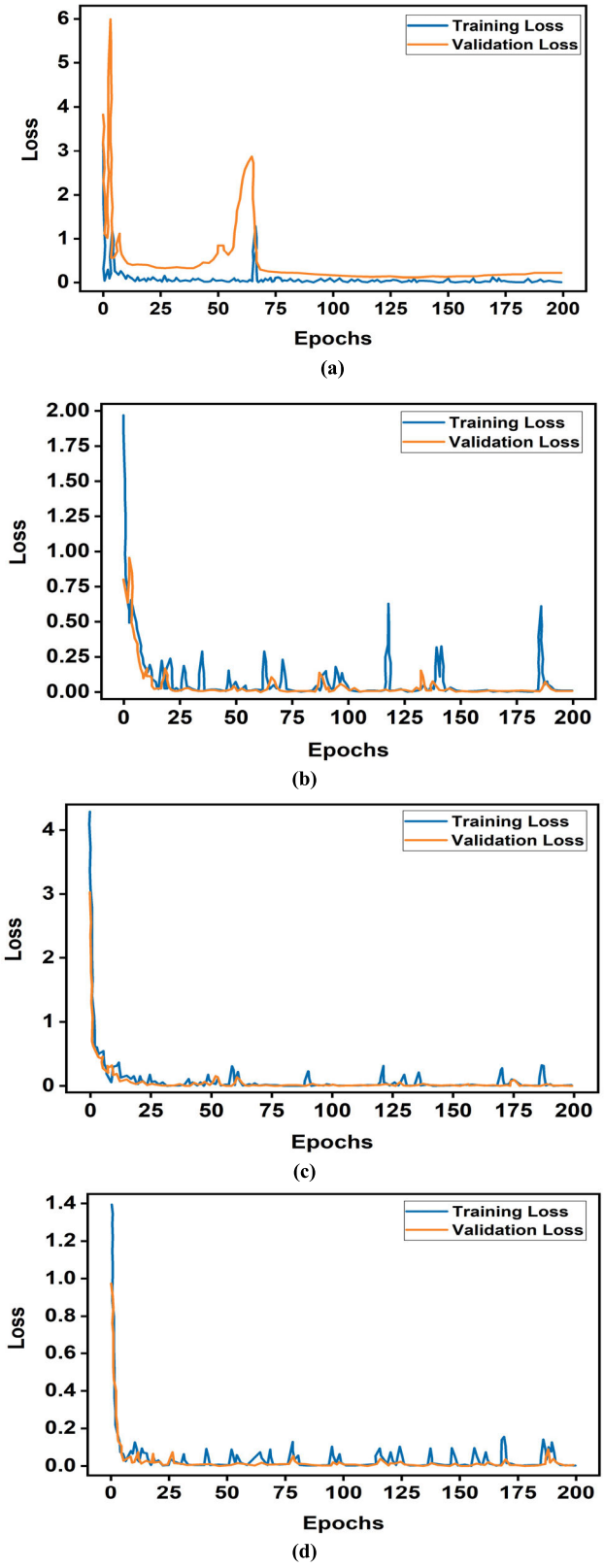

FIGURE 10. Training Vs validation loss: (a) For 200 images data set (b) 400 images data set (c) 600 images data set (d) 800 images data set.

graph with respect to epochs is depicted in Figure 10. It can be observed that when the model is trained by 200 images,

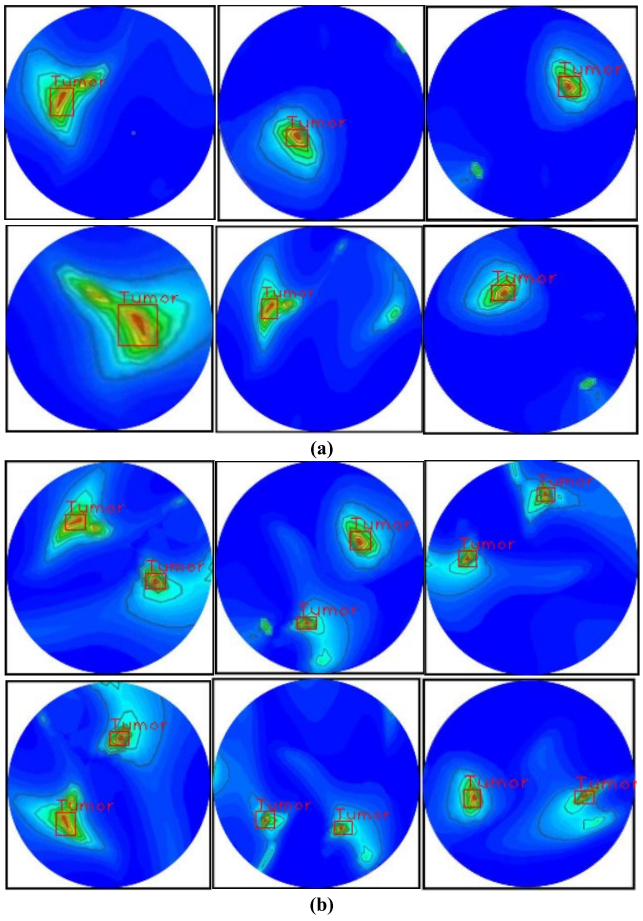

FIGURE 11. Tumor detection in different scenarios from the system: (a) Single tumor detection (b) Double tumors detection.

its validation loss was very high, whereas when the model is trained by 400 images, its validation loss is decreased, but training loss and validation loss are slightly increased in different epochs. In addition, when the model is trained by 600 images, its training and validation loss are lower than the validation loss of 400 images, whereas when the model trained by 800 images, its training and validation loss is very low. Therefore, it can be concluded that the model is more trained by 800 images data set and capable to detect the predicted target objects. The overall observations are presented in Table 2.

C. TUMOR DETECTION IN DIFFERENT SCENARIO

In this section, we discuss the tumor detection results in different scenarios by the trained YOLOv3 model. Different scenarios include (i) images with a single tumor object in the different locations (ii) images with double tumor objects in the different locations as a test set (i.e., 10% images from the final image data set) for detecting the target tumor location in the images. The experimental results are depicted in Figure 11. It can be observed from the detection results in Figure 11, a single tumor with different sizes was successfully detected in their accurate locations, which are shown in

TABLE 2. Overall observations of training and validation loss with different training data sets.

Training Image Data set	Average Training Accuracy (%)	Average Validation Accuracy (%)	Average Training Loss (%)	Average Validation Loss (%)
200	90.21	69.22	25.32	45.63
400	91.35	93.11	20.71	10.61
600	93.82	94.42	18.71	9.62
800	96.74	98.84	14.01	9.21

Figure 11(a). Besides, the double tumors were successfully detected in their precise locations, which are also illustrated in Figure 11(b). In this work, we considered tumor size as the diameter $D = 10$mm,12mm,14mm,15mm,18mm, 20mm, 22mm, 25 mm, but the algorithm could detect any size of the tumor in the images. Finally, it is concluded that the Tumor YOLOv3 model showed potential tumor detection outcomes due to better detection accuracy, F1 score, high training accuracy, and very low validation loss.

VI. CONCLUSION

A YOLOv3 deep neural network model to detect and localize the brain tumor is presented. The portable EM head imaging system is applied to analyze and reconstruct the images. Nine antenna array setup and tissue-mimicking phantom are utilized to collect the scattering parameters, which are later post-processed using the modified delay-multiply-and sum algorithm for image reconstruction. The single generated image contains 416×416 pixels. Fifty sample images are collected from the different scenarios of the developed EM head imaging system, which are later augmented to create a final image data set. The data set consists of 1000 images, including fifty samples, where 80% of them are used for training, and the rest of 20% are used for validation and testing purposes. A large number of 1×1 and 3×3 convolutional layers are used in YOLOv3 architecture, where the Leaky ReLU activation function is used to enlarge the convolutional kernel's step size by diminishing the size of the feature map. The outcome of the presented architecture shows high training and validation accuracy with low training and validation loss. Moreover, the testing phase determines the overall portable EM imaging system's capability and potential of YOLOv3 architecture in detecting and localizing the brain tumor with high accuracy.

REFERENCES

[1] M. L. Schapira and M. W. Dale. *Brain Tumor: Statistics*. Accessed: Apr. 10, 2021. [Online]. Available: https://www.cancer.net/cancer-types/brain-tumor/statistics
[2] A. Hossain, M. T. Islam, M. E. H. Chowdhury, and M. Samsuzzaman, "A grounded coplanar waveguide-based slotted inverted delta-shaped wideband antenna for microwave head imaging," *IEEE Access*, vol. 8, pp. 185698–185724, 2020.
[3] B. J. Mohammed, A. M. Abbosh, S. Mustafa, and D. Ireland, "Microwave system for head imaging," *IEEE Trans. Instrum. Meas.*, vol. 63, no. 1, pp. 117–123, Jan. 2014.
[4] P. A. T. Baltzer, M. Benndorf, M. Dietzel, M. Gajda, I. B. Runnebaum, and W. A. Kaiser, "False-positive findings at contrast-enhanced breast MRI: A BI-RADS descriptor study," *Amer. J. Roentgenol.*, vol. 194, no. 6, pp. 1658–1663, Jun. 2010.
[5] V. Chan and A. Perlas, "Basics of ultrasound imaging," in *Atlas of Ultrasound-Guided Procedures in Interventional Pain Management*. New York, NY, USA: Springer, 2011, pp. 13–19.
[6] M. A. Jacobs, T. S. Ibrahim, and R. Ouwerkerk, "MR imaging: Brief overview and emerging applications," *Radiographics*, vol. 27, no. 4, pp. 1213–1229, 2007.
[7] M. N. Rahman, M. T. Islam, M. Z. Mahmud, and M. Samsuzzaman, "Compact microstrip patch antenna proclaiming super wideband characteristics," *Microw. Opt. Technol. Lett.*, vol. 59, no. 10, pp. 2563–2570, Oct. 2017.
[8] A. Hossain, M. T. Islam, M. T. Islam, M. E. H. Chowdhury, H. Rmili, and M. Samsuzzaman, "A planar ultrawideband patch antenna array for microwave breast tumor detection," *Materials*, vol. 13, no. 21, p. 4918, Nov. 2020.
[9] A. S. M. Alqadami, K. S. Bialkowski, A. T. Mobashsher, and A. M. Abbosh, "Wearable electromagnetic head imaging system using flexible wideband antenna array based on polymer technology for brain stroke diagnosis," *IEEE Trans. Biomed. Circuits Syst.*, vol. 13, no. 1, pp. 124–134, Feb. 2019.
[10] A. Hossain, M. T. Islam, A. F. Almutairi, M. S. J. Singh, K. Mat, and M. Samsuzzaman, "An octagonal ring-shaped parasitic resonator based compact ultrawideband antenna for microwave imaging applications," *Sensors*, vol. 20, no. 5, p. 1354, Mar. 2020.
[11] R. Inum, M. M. Rana, K. N. Shushama, and M. A. Quader, "EBG based microstrip patch antenna for brain tumor detection via scattering parameters in microwave imaging system," *Int. J. Biomed. Imag.*, vol. 2018, pp. 1–12, Feb. 2018.
[12] M. S. Islam, M. T. Islam, A. Hoque, M. T. Islam, N. Amin, and M. E. H. Chowdhury, "A portable electromagnetic head imaging system using metamaterial loaded compact directional 3D antenna," *IEEE Access*, vol. 9, pp. 50893–50906, 2021.
[13] M. Rokunuzzaman, A. Ahmed, T. C. Baum, and W. S. T. Rowe, "Compact 3-D antenna for medical diagnosis of the human head," *IEEE Trans. Antennas Propag.*, vol. 67, no. 8, pp. 5093–5103, Aug. 2019.
[14] A. Salleh, C. Yang, T. Alam, M. Singh, M. Samsuzzaman, and M. Islam, "Development of microwave brain stroke imaging system using multiple antipodal vivaldi antennas based on raspberry Pi technology," *J. Kejuruteraan*, vol. 32, pp. 1–6, Feb. 2020.
[15] A. Salleh, C. C. Yang, M. S. J. Singh, and M. T. Islam, "Development of antipodal Vivaldi antenna for microwave brain stroke imaging system," *Int. J. Eng. Technol*, vol. 8, no. 3, pp. 162–168, 2019.
[16] R. Scapaticci, J. Tobon, G. Bellizzi, F. Vipiana, and L. Crocco, "Design and numerical characterization of a low-complexity microwave device for brain stroke monitoring," *IEEE Trans. Antennas Propag.*, vol. 66, no. 12, pp. 7328–7338, Dec. 2018.
[17] A. S. M. Alqadami, N. Nguyen-Trong, B. Mohammed, A. E. Stancombe, M. T. Heitzmann, and A. Abbosh, "Compact unidirectional conformal antenna based on flexible high-permittivity custom-made substrate for wearable wideband electromagnetic head imaging system," *IEEE Trans. Antennas Propag.*, vol. 68, no. 1, pp. 183–194, Jan. 2020.
[18] I. Merunka, A. Massa, D. Vrba, O. Fiser, M. Salucci, and J. Vrba, "Microwave tomography system for methodical testing of human brain stroke detection approaches," *Int. J. Antennas Propag.*, vol. 2019, pp. 1–9, Mar. 2019.
[19] A. T. Mobashsher and A. M. Abbosh, "Compact 3-D slot-loaded folded dipole antenna with unidirectional radiation and low impulse distortion for head imaging applications," *IEEE Trans. Antennas Propag.*, vol. 64, no. 7, pp. 3245–3250, Jul. 2016.
[20] M. T. Islam, M. Z. Mahmud, M. T. Islam, S. Kibria, and M. Samsuzzaman, "A low cost and portable microwave imaging system for breast tumor detection using UWB directional antenna array," *Sci. Rep.*, vol. 9, no. 1, pp. 1–13, Dec. 2019.
[21] M. Rokunuzzaman, M. Samsuzzaman, and M. T. Islam, "Unidirectional wideband 3-D antenna for human head-imaging application," *IEEE Antennas Wireless Propag. Lett.*, vol. 16, pp. 169–172, 2017.
[22] Z. Sobhaninia, S. Rezaei, A. Noroozi, M. Ahmadi, H. Zarrabi, N. Karimi, A. Emami, and S. Samavi, "Brain tumor segmentation using deep learning by type specific sorting of images," 2018, *arXiv:1809.07786*. [Online]. Available: http://arxiv.org/abs/1809.07786
[23] J. A. T. Vasquez, R. Scapaticci, G. Turvani, G. Bellizzi, N. Joachimowicz, B. Duchêne, E. Tedeschi, M. R. Casu, L. Crocco, and F. Vipiana, "Design and experimental assessment of a 2D microwave imaging system for brain stroke monitoring," *Int. J. Antennas Propag.*, vol. 2019, pp. 1–12, May 2019.

[24] S. A. Rezaeieh, A. Zamani, and A. M. Abbosh, "3-D wideband antenna for head-imaging system with performance verification in brain tumor detection," *IEEE Antennas Wireless Propag. Lett.*, vol. 14, pp. 910–914, 2015.
[25] M. A. Ullah, T. Alam, M. S. Alam, S. Kibria, and M. T. Islam, "A unidirectional 3D antenna for biomedical microwave imaging based detection of abnormality in human body," *Microsyst. Technol.*, vol. 24, no. 12, pp. 4991–4996, Dec. 2018.
[26] E. A. Rashed, J. Gomez-Tames, and A. Hirata, "Deep learning-based development of personalized human head model with non-uniform conductivity for brain stimulation," *IEEE Trans. Med. Imag.*, vol. 39, no. 7, pp. 2351–2362, Jul. 2020.
[27] B. Gerazov and R. C. Conceicao, "Deep learning for tumour classification in homogeneous breast tissue in medical microwave imaging," in *Proc. IEEE 17th Int. Conf. Smart Technol. (EUROCON)*, Jul. 2017, pp. 564–569.
[28] D. Lu, N. Polomac, I. Gacheva, E. Hattingen, and J. Triesch, "Human-expert-level brain tumor detection using deep learning with data distillation and augmentation," 2020, *arXiv:2006.12285*. [Online]. Available: http://arxiv.org/abs/2006.12285
[29] H. Mohsen, E.-S. A. El-Dahshan, E.-S. M. El-Horbaty, and A.-B. M. Salem, "Classification using deep learning neural networks for brain tumors," *Future Comput. Informat. J.*, vol. 3, no. 1, pp. 68–71, 2018.
[30] W. Shao and Y. Du, "Microwave imaging by deep learning network: Feasibility and training method," *IEEE Trans. Antennas Propag.*, vol. 68, no. 7, pp. 5626–5635, Jul. 2020.
[31] A. Işın, C. Direkoğlu, and M. Şah, "Review of MRI-based brain tumor image segmentation using deep learning methods," *Procedia Comput. Sci.*, vol. 102, pp. 317–324, Jan. 2016.
[32] P. Mojabi, V. Khoshdel, and J. Lovetri, "Tissue-type classification with uncertainty quantification of microwave and ultrasound breast imaging: A deep learning approach," *IEEE Access*, vol. 8, pp. 182092–182104, 2020.
[33] H. M. Yao, L. Jiang, and W. E. I. Sha, "Enhanced deep learning approach based on the deep convolutional encoder–decoder architecture for electromagnetic inverse scattering problems," *IEEE Antennas Wireless Propag. Lett.*, vol. 19, no. 7, pp. 1211–1215, Jul. 2020.
[34] V. Khoshdel, M. Asefi, A. Ashraf, and J. LoVetri, "Full 3D microwave breast imaging using a deep-learning technique," *J. Imag.*, vol. 6, no. 8, p. 80, Aug. 2020.
[35] M. Ambrosanio, S. Franceschini, F. Baselice, and V. Pascazio, "Machine learning for microwave imaging," in *Proc. 14th Eur. Conf. Antennas Propag. (EuCAP)*, Mar. 2020, pp. 1–4.
[36] P. Shah, G. Chen, and M. Moghaddam, "Learning nonlinearity of microwave imaging through deep learning," in *Proc. IEEE Int. Symp. Antennas Propag., USNC/URSI Nat. Radio Sci. Meeting*, Jul. 2018, pp. 699–700.
[37] P. Shah and M. Moghaddam, "Super resolution for microwave imaging: A deep learning approach," in *Proc. IEEE Int. Symp. Antennas Propag., USNC/URSI Nat. Radio Sci. Meeting*, Jul. 2017, pp. 849–850.
[38] A. Chaurasia and E. Culurciello, "LinkNet: Exploiting encoder representations for efficient semantic segmentation," in *Proc. IEEE Vis. Commun. Image Process. (VCIP)*, Dec. 2017, pp. 1–4.
[39] H. Dong, G. Yang, F. Liu, Y. Mo, and Y. Guo, "Automatic brain tumor detection and segmentation using U-Net based fully convolutional networks," in *Proc. Annu. Conf. Med. Image Understand. Anal.*, 2017, pp. 506–517.
[40] A. T. Mobashsher and A. M. Abbosh, "Three-dimensional human head phantom with realistic electrical properties and anatomy," *IEEE Antennas Wireless Propag. Lett.*, vol. 13, pp. 1401–1404, 2014.
[41] J. Redmon, S. Divvala, R. Girshick, and A. Farhadi, "You only look once: Unified, real-time object detection," in *Proc. IEEE Conf. Comput. Vis. Pattern Recognit. (CVPR)*, Jun. 2016, pp. 779–788.
[42] J. Redmon and A. Farhadi, "YOLOv3: An incremental improvement," 2018, *arXiv:1804.02767*. [Online]. Available: http://arxiv.org/abs/1804.02767
[43] J. Redmon and A. Farhadi, "YOLO9000: Better, faster, stronger," in *Proc. IEEE Conf. Comput. Vis. Pattern Recognit. (CVPR)*, Jul. 2017, pp. 7263–7271.
[44] H. Huang, D. Sun, R. Wang, C. Zhu, and B. Liu, "Ship target detection based on improved YOLO network," *Math. Problems Eng.*, vol. 2020, pp. 1–10, Aug. 2020.

AMRAN HOSSAIN (Member, IEEE) was born in Chandpur, Bangladesh, in 1981. He received the B.Sc. and M.Sc. degrees in computer science and engineering from the Dhaka University of Engineering & Technology, Gazipur, Bangladesh, in 2009 and 2015, respectively. He is currently pursuing the Ph.D. degree with Universiti Kebangsaan Malaysia (UKM), Malaysia. From September 2012 to July 2015, he worked as a Lecturer with the Dhaka University of Engineering & Technology, Gazipur. From July 2015 to September 2019, he worked as an Assistant Professor with the Dhaka University of Engineering & Technology, Gazipur. He has published about nine research journal articles and two conference papers. Also, he wrote a few book chapters on various topics related to computer programming language, information analysis, and design and computer graphics. His research interests include wireless communication antenna design, electromagnetic imaging, machine learning, deep learning, and cognitive radio networks.

MOHAMMAD TARIQUL ISLAM (Senior Member, IEEE) is currently a Professor with the Department of Electrical, Electronic and Systems Engineering, Universiti Kebangsaan Malaysia (UKM), and a Visiting Professor with the Kyushu Institute of Technology, Japan. He is the author and the coauthor of about 500 research journal articles, nearly 200 conference papers, and a few book chapters on various topics related to antennas, metamaterials, and microwave imaging with 22 inventory patents filed. Thus far, his publications have been cited 7300 times and his H-index is 41 (Source: Scopus). His Google scholar citation is 11 000 and H-index is 48. He was a recipient of more than 40 research grants from the Malaysian Ministry of Science, Technology and Innovation, the Ministry of Education, the UKM research grant, and international research grants from Japan, Saudi Arabia, and Kuwait. His research interests include communication antenna design, metamaterial, satellite antennas, and microwave imaging. He had been serving as an Executive Committee Member for IEEE AP/MTT/EMC Malaysia Chapter, from 2019 to 2020, the Chartered Professional Engineer (CEng), a Fellow of IET, U.K., and a Senior Member of IEICE, Japan. He received several International Gold Medal awards, the Best Invention in Telecommunication Award for his research and innovation, and best researcher awards from UKM. He was a recipient of 2018, 2019, and 2020 IEEE AP/MTT/EMC Malaysia Chapter, Excellent Award. He also won the best innovation award and the Best Research Group in ICT niche by UKM, in different years. He was also a recipient of Publication Award from the Malaysian Space Agency, in several years. He has supervised about 30 Ph.D. theses, 20 M.Sc. theses, and has mentored more than ten postdocs and visiting scholars. He has developed the Antenna Measurement Laboratory which includes antenna design and measurement facility till 40 GHz. He was an Associate Editor of IET *Electronics Letter*. He also serves as the Guest Editor for *Sensors* journal, and an Associate Editor for IEEE Access.

MOHAMMAD SHAHIDUL ISLAM (Graduate Student Member, IEEE) was born in Brahmanbaria, Bangladesh, in 1993. He received the B.Tech. degree (Hons.) in software engineering from Infrastructure University Kuala Lumpur. He is currently pursuing the M.Sc. degree in electrical and electronic engineering with Universiti Kebangsaan Malaysia (UKM), Malaysia. He is also a Graduate Research Assistant with the Department of Electrical, Electronic, and Systems Engineering, UKM. He is also an ICT Research Fellow with the Ministry of Posts, Telecommunications and Information Technology, Bangladesh. He has authored or coauthored a number of refereed journal articles and conference papers. His research interests include the Internet of Things, antenna and wave propagation, wireless communication, and electromagnetic imaging. He was a recipient of IEEE AP/MTT/EMC Best Paper Award 2019 and 2020.

MUHAMMAD E. H. CHOWDHURY (Senior Member, IEEE) received the B.Sc. and M.Sc. degrees (Hons.) from the Department of Electrical and Electronics Engineering, University of Dhaka, Bangladesh, and the Ph.D. degree from the University of Nottingham, U.K., in 2014. He worked as a Postdoctoral Research Fellow and the Hermes Fellow with the Sir Peter Mansfield Imaging Centre, University of Nottingham, U.K. He is currently working as a full-time Faculty Member with the Electrical Engineering Department, Qatar University. Prior to joining Qatar University, he worked in several universities of Bangladesh. He has a patent and published around 60 peer-reviewed journal articles, conference papers, and two book chapters. His current research interests include biomedical instrumentation, signal processing, wearable sensors, medical image analysis, machine learning, embedded system design, and simultaneous EEG/fMRI. He is also running several NPRP and UREP grants from QNRF and internal grants from Qatar University along with academic and government projects. He has been involved in EPSRC, ISIF, and EPSRC-ACC grants along with different national and international projects. He has worked as a consultant for the projects entitled, ''Driver Distraction Management Using Sensor Data Cloud (2013–2014, Information Society Innovation Fund (ISIF) Asia).'' He received ISIF Asia Community Choice Award 2013 for project entitled ''Design and Development of Precision Agriculture Information System for Bangladesh.'' He has recently won COVID-19 dataset award for his contribution to fight against COVID-19. He is also an Active Member of IEEE, British Radiology, Institute of Physics, ISMRM, and HBM. He is also serving as an Associate Editor for IEEE Access and Review Editor for *Frontiers in Neuroscience*.

ALI F. ALMUTAIRI (Senior Member, IEEE) received the B.S. degree in electrical engineering from the University of South Florida, Tampa, FL, USA, in 1993, and the M.S. and Ph.D. degrees in electrical engineering from the University of Florida, Gainesville, FL, USA, in 1995 and 2000, respectively. He had been the Dean of Admission and Registration with Kuwait University, from July 2018 to December 2020. He has served as the Vice Dean of Academic Affairs for the College of Engineering and Petroleum, Kuwait University, from March 2016 to July 2018. He has also served as the Chairperson for the Electrical Engineering Department, Kuwait University, from March 2007 to September 2011, and has also served as the Graduate Program Director for the Electrical Engineering Department, Kuwait University, from September 2015 to September 2016. He is currently a Professor with the Electrical Engineering Department. His current research interests include multiuser detection, wireless networks, antenna design, and current and future cellular networks performance issues. He is also a member of other professional societies. In December 1993, he was awarded a Full Scholarship from Kuwait University to pursue his graduate studies. He has also served/serving as an associate editor and a reviewer for many technical publications.

QUTAIBA A. RAZOUQI (Member, IEEE) received the B.Sc. degree in electrical engineering (in communication) and the M.Sc. degree in optical communications from the University of Kent at Canterbury, U.K., in 1991 and March 1993, respectively, and the Ph.D. degree in computer science and engineering (communication networks) from Arizona State University, Tempe, AZ, USA, in 1999. He has been serving as the Director for the Kuwait University Construction Program, since January 2014, which is responsible of overlooking the construction of the new campus for Kuwait University. He is currently an Assistant Professor with the Electrical Engineering Department, Kuwait University. His current research interests include high speed networks, ad-hoc and sensor networks, social networking, cloud networking, network security, and the IoT and big data. He is also a member of other professional societies. In June 1991, he has been awarded a Full Scholarship from Kuwait University to pursue his graduate studies.

NORBAHIAH MISRAN (Senior Member, IEEE) received the B.Eng. degree in electrical, electronic and system engineering from Universiti Kebangsaan Malaysia (UKM), in 1999, and the Ph.D. degree from the Queen's University of Belfast, U.K., in 2004. She started her career as a Tutor, in 1999, at the Department of Electrical, Electronic and System Engineering, UKM. She later has been appointed as a Lecturer, in 2004, an Associate Professor, in 2009, and later as a Professor, in 2012, with the Department of Electrical, Electronic and System Engineering. She is the author and coauthor of more than 400 research articles in microwave device and systems and engineering education. Her research interests include microwave device and systems particularly in broadband microstrip antennas, reconfigurable antennas, reflect array antennas, and metamaterials. She is also conducting some research in engineering education field.